Review Article

Yong Wang*, Takeo Ohsawa, Fahad Alnjiman, Jean-Francois Pierson, and Naoki Ohashi

Electrical properties of zinc nitride and zinc tin nitride semiconductor thin films toward photovoltaic applications

https://doi.org/10.1515/htmp-2022-0028
received September 30, 2021; accepted February 18, 2022

Abstract: Zn_3N_2 (ZN) and $ZnSnN_2$ (ZTN) are a promising class of nitride semiconductors for photovoltaic and light-emitting-diode applications due to their particular electrical and optical properties, elemental abundance and non-toxicity. So far, most of the experimental results show the degenerate carrier concentration. However, we find that low-temperature growth of these films in a chamber with ultra-high background vacuum can attain a non-degenerate electrical conductivity. This work provides the recent progress of the electrical properties of ZN and ZTN semiconductor thin films. The origins for the high carrier concentrations in ZN and ZTN have been discussed, demonstrating that non-intentional oxygen and hydrogen-related defects play significant roles in such high carrier concentrations. The strategies to suppress the carrier concentrations have also been addressed, such as ultra-high vacuum conditions and low temperature growth.

Keywords: II–IV-N_2 semiconductors, thin films, defects, microstructure, electrical properties

*** Corresponding author: Yong Wang,** International Center for Young Scientists, National Institute for Materials Science, Tsukuba, Ibaraki 305-0044, Japan; School of Space Science and Physics, Shandong University, Weihai 264209, China, e-mail: wang.yong06@sdu.edu.cn

Takeo Ohsawa, Naoki Ohashi: Research Center for Functional Materials, National Institute for Materials Science, Tsukuba, Ibaraki 305-0044, Japan

Fahad Alnjiman: Département Chimie et Physique des Solides et des Surfaces, Institut Jean Lamour, UMR 7198-CNRS, Université de Lorraine, Nancy 54011, France; Department of Physics and Astronomy, College of Science, King Saud University, Riyadh 11451, Saudi Arabia

Jean-Francois Pierson: Département Chimie et Physique des Solides et des Surfaces, Institut Jean Lamour, UMR 7198-CNRS, Université de Lorraine, Nancy 54011, France

1 Introduction

Zn_3N_2 (ZN) is an attractive nitride composed of only earth-abundant elements. The small effective mass of 0.08 m_o (m_o is the free electron mass) indicates the potential high electron mobility [1,2]. In addition, a theoretical band gap of 0.84 eV matches the required ones to achieve a theoretically high conversion efficiency in single junction solar cells referring to the Shockley–Queisser limit [3]. These features render ZN to be a promising material for thin-film photovoltaic absorber. However, most of the experimental results show quite high carrier concentrations (10^{18}–10^{21} cm^{-3}) even without intentional doping [4–8]. Such degenerate electrical properties may prevent its semiconducting applications.

Wurtzite-derived II–IV-N_2 semiconductors, such as $ZnSnN_2$ (ZTN) and $ZnGeN_2$, have also received increasing interest for their great potential to complement group-III nitrides (like GaN, AlN and InN) as optoelectronic materials [9–15]. From the viewpoints of both economic and ecological perspectives, II–IV-N_2 semiconductors composed of Zn, Sn and Ge are highly attractive, due to the low cost of these elements than Ga and In, as well as their more mature recycling infrastructures [11]. On the other hand, these II–IV-N_2 semiconductors are structurally analogous to the group-III nitrides [16,17], which is beneficial to the growth of epitaxial heterojunctions by the existing technologies and substrates. In addition, some physical properties of II–IV-N_2 semiconductors are comparable or even superior to group-III nitrides. A typical example among various II–IV-N_2 semiconductors is ZTN, which is composed of only earth-abundant elements. The theoretical electron and hole effective masses of ZTN are 0.11 and 1.96 m_0, respectively [2], whereas the same calculation approach gives the electron and hole effective masses of 0.18 and 1.97 m_0 for GaN, respectively [2]. Besides, the medium band gap (1.4–1.8 eV) of ZTN may make up the drawbacks of indium segregation and phase separation in $In_xGa_{1-x}N$ with similar band gap [10,18,19].

These fascinating properties of ZTN qualify it to be a very promising low-cost material for photovoltaic and light-emitting-diode applications [10,16].

Although various research studies on the ZTN material have been performed for nearly one decade, an obstacle that remains to hinder its semiconducting applications is the high electron concentration (10^{17}–10^{21} cm^{-3}) [9,10,20–22] regardless of ZTN in bulks [23] or in thin films grown by sputtering or molecular beam epitaxy [9,10,24–26]. Joint experimental and theoretical studies reveal that the high carrier concentration of ZTN comes from the large amounts of intrinsic Sn-on-Zn (Sn_{Zn}^{2+}) defects and non-intentional oxygen-on-nitrogen (O_N^+) and/or hydrogen interstitial (H_i^+) impurities, as these donor-type defects have low formation energies [27,28]. Excess Zn content and low temperature growth can suppress these defects partially, yielding the carrier concentration of around 2.7×10^{17} cm^{-3} at room temperature [28]. Obviously, such carrier concentration of ZTN is still inferior to those of group-III nitrides. Quite recently, theoretical calculations on the defect properties of ZTN have shown that the associations between Zn-on-Sn (Zn_{Sn}^{-2}) and O_N^+/H_i^+ defects yield the defect complexes (like $(Zn_{Sn} + 2O_N)^0$ and $(Zn_{Sn} + 2H_i)^0$) with neutral charge, which are of great value to control the electron concentrations [27,29]. Taking $(Zn_{Sn} + 2H_i)^0$ as an example, the complexing with H_i^+ is exothermic and decreases the formation energy of acceptor-type Zn_{Sn}^{-2} significantly. The energy change from isolated Zn_{Sn}^{-2} and H_i^+ to $(Zn_{Sn} + O_N)^-$ is −1.43 eV and that from isolated $(Zn_{Sn} + O_N)^-$ and H_i^+ to $(Zn_{Sn} + 2H_i)^0$ is −0.73 eV [27]. The couplings between Zn_{Sn}^{-2} and O_N^+ show similar characteristics [29]. Such defect complexes with neutral charge possess quite low formation energy, which can restrain the contribution of donor-type Sn_{Zn}^{2+}, O_N^+, H_i^+ and nitrogen vacancy (V_N^+) defects effectively [29]. The modeling of electron scattering mechanism of ZTN also supports such an hypothesis regarding the defect complex $(Zn_{Sn} + 2H_i)^0$ [30]. These results seem to show that the joint cation and anion sublattice has a significant influence on the electrical properties of ZTN.

Although ZTN and ZN have been widely studied, the results are still subject to controversial issues and ambiguities. Particularly, their degenerate electrical properties seriously frustrate their applications. Hence, a critical look at their electrical properties is highly desirable. In this work, we try to summarize the recent progress of the electrical transport mechanisms of ZTN and ZN, in order to reveal their origins of the degenerate carrier concentrations.

2 Experimental details

Zn_3N_2 thin films were grown on Si (100) and glass substrates by reactive magnetron sputtering in an ultra-high vacuum (UHV) chamber (background pressure of 10^{-7} Pa, Eiko) connected with a load-lock chamber (background pressure of 10^{-5} Pa). High purity N_2 (Grade 1, 99.99995% purity) was used as the sole reactive gas with a partial pressure of 0.78 Pa. A radio frequency (RF) power supply (Kyosan) with a power of 55 W was connected to a Zn target (2 in. diameter with a purity of 99.99%). Various substrate temperatures (near room temperature, 100 and 150°C) were employed to grow the Zn_3N_2 thin films. The thickness of thin films was around 400–430 nm. After the depositions, Zn_3N_2 thin films were transferred and stored in the load-lock chamber to prevent the pollution in atmospheric environments [31]. In the following, these Zn_3N_2 thin films are referred to as "ZN."

Two chambers with background vacuum of 10^{-3} and 10^{-7} Pa were used to grow zinc tin nitride thin films. The Zn/(Zn + Sn) was determined by electron probe microanalyzer (EPMA, JEOL 8530F) and energy dispersive X-ray spectroscopy (EDS, JEOL JSM-7001F). The O anion composition (at%) is estimated by the EPMA using various standard species (like metallic Fe_4N, MgO, Zn and Sn). For the thin films grown in the chamber with the poor background vacuum of 10^{-3} Pa, the O contents are 2.3–5.7%. In the following, these oxynitride thin films are referred to as "ZTNO." On the contrary, the O contents of ZTN thin films deposited in the UHV chamber with background vacuum of 10^{-7} Pa are smaller than the detectable limit, indicating quite a little oxygen contamination. In both cases, thin films were synthesized on glass and Si (100) substrates in high purity N_2 atmosphere and no intentional heating was applied to the substrates. Thus, the substrate temperature was at near room temperature. ZTNO thin films were deposited by reactive co-sputtering of Zn and Sn metal targets (2 in. diameter with a purity of 99.99%) connected to two pulsed DC supplies (Pinnacle + Advanced Energy), respectively. A fixed voltage of 440 V is applied in the Sn target, while the voltage on the Zn target is tuned from 240 to 300 V to achieve the various cation compositions of ZTNO thin films. During the growth process of ZTNO thin films, a nitrogen flow rate of 60 sccm was used and the total pressure was kept at 1 Pa. The thickness of ZTNO thin films is 1.7–2.2 μm. More details about the growth of ZTNO films are described in ref. [25]. On the other hand, two RF power supplies (Kyosan) were used to grow ZTN thin films.

Zn and Sn metal targets were inclined at an angle of 45°. The input powers on the Sn and Zn targets were tuned at 20–35 and 30–80 W, respectively. ZTN thin films were deposited at various substrate temperatures, including near room temperature, 250 and 350°C. During the growth process of ZTN thin films, the N_2 partial pressure and the total sputtering pressure are 1.56 and 1.59 Pa, respectively. More details concerning the growth of ZTN-U thin films can be found in ref. [28]. The phase structures of thin films have been checked by the X-ray diffraction (XRD, Bruker D8 Advance with Cu $K_{\alpha 1}$ radiation). Electrical properties were determined by resistivity and Hall-effect measurements (Toyo Corp. Resitest 8300) using a van der Pauw configuration. The microstructure was investigated by a transmission electron microscopy (TEM, JEOL 2100F). For this purpose, TEM specimens were prepared by diamond tip cleave.

A series of ZTNO thin films with various Zn/(Zn + Sn) compositions have been deposited on glass substrates by sputtering chamber with poor background vacuum of 10^{-3} Pa. Here it is worth noting that the intentional inlet of oxygen gas into the sputtering chamber is detrimental to form the crystallized ZTN, as the sputtered Zn and Sn atoms easily react with oxygen to produce the oxide phases. But the poor background vacuum (like 10^{-3} Pa) may keep the crystal structure of nitride and provide certain amount of oxygen to generate the oxynitride thin films simultaneously. On the contrary, UHV (like 10^{-7} Pa) will suppress the formation of oxynitride thin films due to quite a little content of oxygen.

3 Electrical and defect properties of ZN thin films

ZN thin films have been grown at different substrate temperatures (near room temperature, 100 and 150°C) by reactive magnetron sputtering in an UHV chamber. The *n*-type conductivity and carrier concentration (n) in these ZN thin films have been identified by standard Hall-effect measurements. However, it is found that the growth temperature has a significant influence on the magnitude of n (Figure 1). The value of n at 300 K (n_{300K}) of the ZN thin films deposited at near room temperature is 1.6×10^{17} cm^{-3}. In the cases of growth temperatures of 100 and 150°C, n_{300K} of 8.2×10^{17} and 1.1×10^{19} cm^{-3} has been achieved, respectively, indicating that n increases with an increase of the growth temperature. The analyses of carrier concentration as a function of temperature give an activation energy of 0.29 eV in the ZN thin film grown at near room

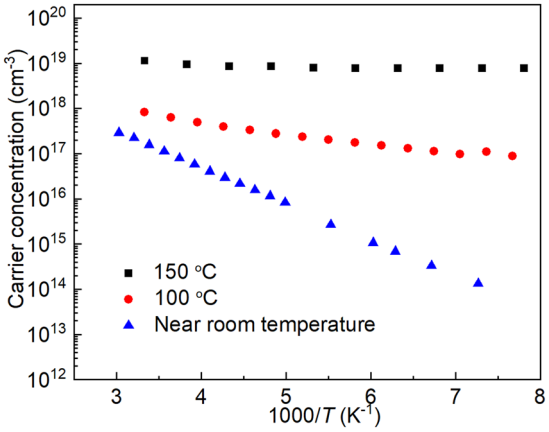

Figure 1: Temperature dependence of carrier concentration of Zn_3N_2 thin films grown at different temperatures (near room temperature, 100 and 150°C) (reprinted from ref. [31]).

temperature, demonstrating the non-degenerate characteristics. These results seem to show that low temperature deposition yields non-degenerate ZN thin films, while elevating the growth temperature generates significantly larger n [31].

Checking the XRD patterns of these ZN thin films grown at different substrate temperatures (Figure 2) [31], it is found that all thin films exhibit the polycrystalline diffraction features, without amorphous characteristics, even for thin films grown at near room temperature. Elevating the growth temperature from near room temperature to 150°C results in significant enhancement of (400) diffraction intensities in these ZN thin films, demonstrating a preferred growth at higher temperatures. However, the full width at half maximum (FWHM) of (400) diffraction

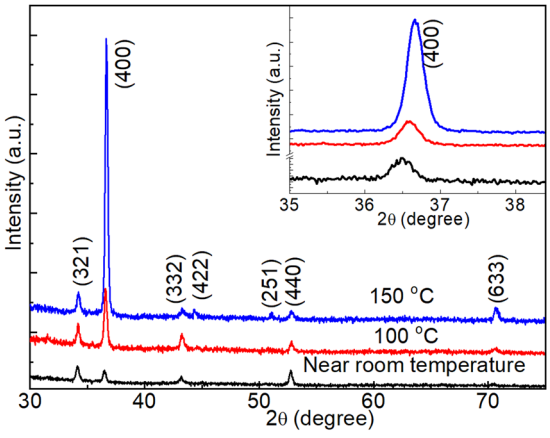

Figure 2: XRD patterns of ZN thin films on glass substrates with temperatures of near room temperature, 100 and 150°C. The inset shows the magnified (400) diffraction peaks of the corresponding ZN thin films (reprinted from ref. [31]).

peaks just slightly decrease from 0.30° (near room temperature), 0.28° (100°C) to 0.26° (150°C), implying that the coherent lengths of these ZN thin films slightly increase when increasing the substrate temperature by referring to the Scherrer equation. These XRD features seem to indicate that the slight increase of grain boundary effect at near room temperature growth is not the dominant source for the remarkable reduction of carrier concentration [31].

Analyses of defect concentrations based on the defect formation energies estimated from the first-principle calculations indicate that all the native defects (such as V_N^+ and Zn_i^{2+}) are not responsible for the high carrier concentrations, as their density is far too small. However, unintentional oxygen-on-nitrogen (O_N^+) and/or hydrogen interstitial (H_i^+) defects may act as dominant donors in the ZN thin films [31,32]. For the comparisons between calculations and experiments, we assume a singly ionized donor (O_N^+, H_i^+ or both of them) with $N = 16$ (number of nitrogen sites in the unit cell) and determine E_D, $q = +1$ (the formation energy of defect D in charge state q) by fitting to the experimental n_{300K} of ZN thin films. As seen in Figure 3, the theoretical concentration of O_N^+, H_i^+ or both of them (Curve (1)) captures the tendency of the experimental values. Therefore, the remarkable growth temperature dependence of carrier concentration in ZN thin films would be attributed to the Boltzmann distribution of O_N^+/H_i^+ impurities [31].

Referring to such theoretical calculations, the mechanisms behind the reported high n and our tunable n by different growth temperatures in ZN thin films can be qualitatively explained. The background vacuum with residual gas in the chamber may be an important origin for O/H contaminations. A detailed check on the growth conditions and carrier concentration of ZN thin films shows that most of other reported ZN thin films fabricated in non-UHV chamber (background vacuum $>10^{-5}$ Pa) possess relatively high n, where much more amount of O/H impurities may remain. This may be due to the low formation energies of donor-type O_N^+ and H_i^+ in ZN. On the contrary, thin films deposited in UHV conditions (~10^{-7} Pa) in this study exhibit much lower n, as there are less O/H impurities. On the other hand, when the growth temperature of the substrate is increased, the concentrations of O_N^+ and H_i^+ will increase based on the Boltzmann distribution [31]. This could explain the increase of n_{300} by 2 orders of magnitude when increasing the growth temperature from near room temperature to 150°C (as shown in Figure 1).

4 Electrical properties of ZTN thin films grown in an UHV chamber

The electrical properties of zinc tin nitride ($Zn_{1+x}Sn_{1-x}N_2$) thin films grown by reactive sputtering in an UHV chamber have been investigated. The fractional Zn atomic percent (at%) to the total cation (at%) in ZTN thin films, expressed by Zn/(Zn + Sn), was used to describe the off-stoichiometry of Zn element. Figure 4 shows the $n_{300\ K}$ of ZTN thin films with various cation compositions deposited at near room temperature, 250 and 350°C. It is demonstrated that both Zn-rich content and low-temperature growth are beneficial for suppressing the carrier concentration. The lowest n_{300K}

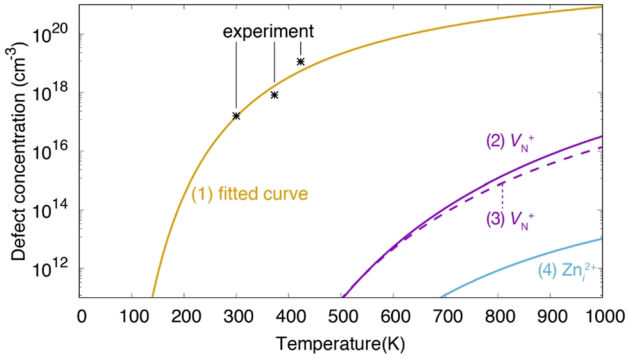

Figure 3: Temperature dependence of defect concentrations in Zn_3N_2. Curve (1) shows the concentrations of O_N^+, H_i^+ or both of them fitted to the experimental $n_{300\ K}$ of Zn_3N_2 thin films grown at near room temperature. Curves (2) and (3) represent the concentrations of V_N^+ calculated by using the formation free energies depending on the temperature and the formation energies of the competing phases at 0 K, respectively. Same data as (2) but for Zn_i^{2+} is shown as curve (4) (reprinted from ref. [31]).

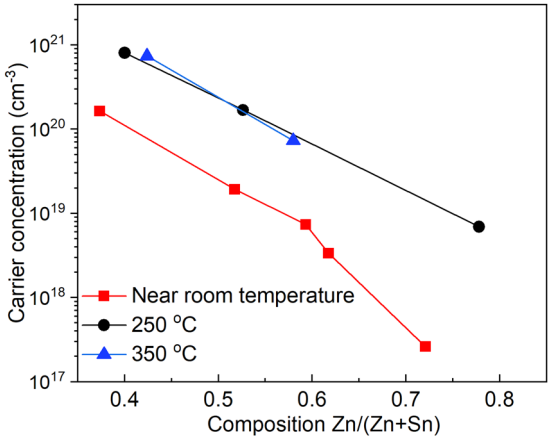

Figure 4: Carrier concentration as a function of cation composition Zn/(Zn + Sn) in ZTN thin films deposited at various temperatures (near room temperature, 250 and 350°C) (reprinted from ref. [28]).

of 2.7×10^{17} cm^{-3} was achieved in thin films grown at near room temperature with a composition of Zn/(Zn + Sn) = 0.72, which are in contrast to the previously formed degenerate thin films with much higher carrier concentrations [28]. As shown in Figure 4, thin films with Zn-poor (Sn-rich) contents exhibit larger carrier concentrations. This may come from the high amount of donor-type Sn_{Zn}^{2+} defects, as the calculations show the much lower formation energy for Sn_{Zn}^{2+} [27]. Such tunable electrical properties by Zn content are well consistent with the recent first-principle calculation, suggesting that excess Zn can reduce the amount of native donor-type Sn_{Zn}^{2+} defects [27], while low-temperature growth can decrease the concentrations of unintentional donor-type oxygen-on-nitrogen (O_N^+) and/or hydrogen interstitial (H_i^+) impurities [28].

5 A comparative study on ZTN thin films grown in UHV and non-UHV sputtering chambers

A magnetron sputtering chamber with a poor background vacuum of 10^{-3} Pa is also used to grow zinc tin nitride thin films, in order to perform a comparative study with thin films deposited in the UHV chamber with a background vacuum of 10^{-7} Pa. The purposes are to develop a comprehensive picture on tuning the electrical properties of zinc tin nitride thin films with excess Zn and O compositions.

First, we show the XRD results of ZTNO and ZTN thin films. The XRD patterns of ZTNO and ZTN thin films with different Zn/(Zn + Sn) compositions are shown in Figure 5(a) and (b), respectively. In addition, a diffraction pattern of ZnO thin film grown in the poor vacuum chamber with the O_2 and Ar flow rates of 7 and 25 sccm is depicted as a reference in Figure 5(a). Referring to the theoretical electronic structures of ZTN, it is seen that orthorhombic and wurtzite phases possess the direct band gap of 1.4 and 0.4 eV, respectively [19,27]. However, our ZTNO and ZTN thin films show the optical band gap of 1.3–1.6 eV, implying that the predominant phase of these thin films should be orthorhombic, rather than wurtzite. While the theoretical diffraction patterns of orthorhombic ZTN and wurtzite ZnO are presented in Figure 5(c), which are acquired from the Materials Database of NREL (http://materials.nrel.gov) [33]. Since the energetically favorable orthorhombic ZTN derives from the wurtzite structure, the crystallographic characteristics of ZTN and ZnO are quite similar, yielding the close

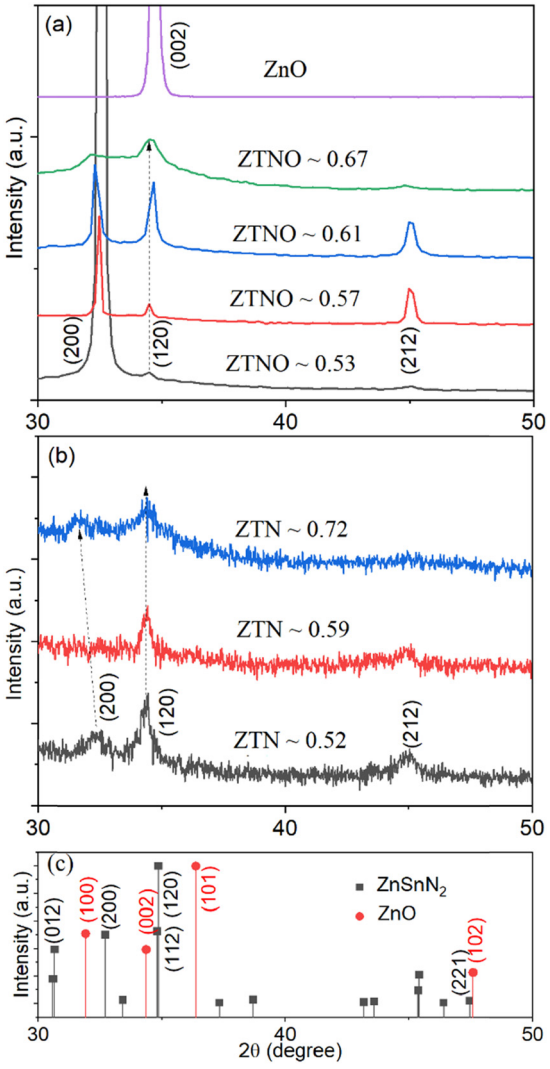

Figure 5: (a) X-ray diffraction patterns of ZTNO thin films on glass substrates with various Zn/(Zn + Sn) (0.53, 0.57, 0.61 and 0.65) compositions grown by a sputtering chamber with the background vacuum of 10^{-3} Pa. ZnO thin film grown by the same chamber is plotted for comparison. (b) X-ray diffraction patterns of ZTN thin films with various Zn/(Zn + Sn) (0.52, 0.59 and 0.72) compositions grown by a sputtering chamber with the background vacuum of 10^{-7} Pa. (c) Theoretical diffraction patterns of $ZnSnN_2$ and ZnO (authors' original work).

diffraction peaks (like ZTN (120) and ZnO (002), ZTN (200) and ZnO (100)), as shown in Figure 5(c). Looking at Figure 5(a), the (200) diffraction peaks of ZTNO shift to a lower angle when increasing the Zn/(Zn + Sn) content, whereas the (120) diffraction peaks have a tendency to move to a larger angle. At high Zn/(Zn + Sn) composition, the (120) diffraction peaks of ZTNO thin films are much more close to the (002) diffraction peak of ZnO thin film. Unlike ZTNO films, ZTN thin films with different Zn/(Zn + Sn) contents do not exhibit such shift on (120) diffraction

peaks, rather nearly constant (120) peaks regardless of Zn/(Zn + Sn) compositions. These results seem to demonstrate that ZTNO thin films with high Zn content show some crystallographic features of ZnO thin films.

Next, dramatic difference in electrical properties between ZTNO and ZTN thin films was observed. Figure 6 shows resistivity (ρ) of ZTNO and ZTN thin films at 300 K. As shown in Figure 6, the ρ of nearly perfect cation composition ZTNO ~0.53 Zn/(Zn + Sn) thin film is quite close to that of ZTN ~ 0.52 Zn/(Zn + Sn) thin film. However, their mobility and carrier concentrations exhibit notable discrepancies. The Hall mobilities (μ_H) of ZTNO ~0.53 Zn/(Zn + Sn) and ZTN ~ 0.52 Zn/(Zn + Sn) thin films are 0.27 and 1.9 $cm^2 \cdot V^{-1} \cdot s^{-1}$, respectively. Their corresponding values of n are 5.9×10^{19} and 1.9×10^{19} cm^{-3}, respectively. The O anion composition of ZTNO ~ 0.53 Zn/(Zn + Sn) is around 2.3%, whereas the O content of ZTN ~ 0.52 Zn/(Zn + Sn) is smaller than the detectable limit. Thus, these experimental results seem to show that oxygen impurities from the residual gas in the growth chamber increase n and simultaneously suppress μ_H in the nearly stoichiometric ZTNO thin film. This agrees well with the theoretical prediction that O_N^+ point defects with low formation energies act as shallow donors in ZTN with perfect 0.5 Zn/(Zn + Sn) composition [27,29].

Increasing the Zn/(Zn + Sn) compositions, the ρ of ZTN thin films just enhance a little at Zn-rich compositions, from 0.167 (Zn/(Zn + Sn) ~ 0.52) to 8.72 Ω·cm (Zn/(Zn + Sn) ~ 0.72). As reported in our previous work, the slight increase of ρ of ZTN thin films at Zn-rich compositions is mainly due to the reduction of n and the enhancement of μ_H [28].

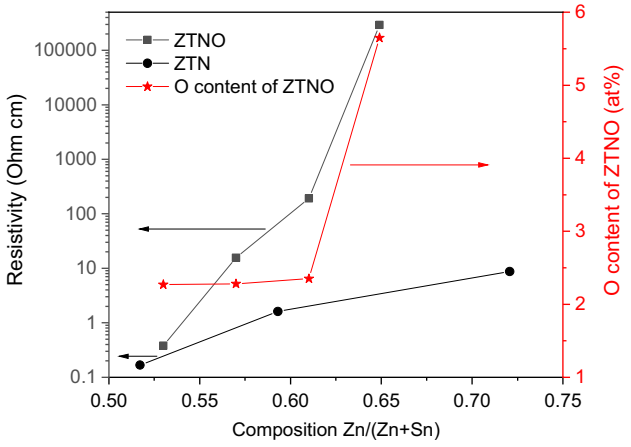

Figure 6: Resistivity vs cation composition Zn/(Zn + Sn) of ZTNO and ZTN thin films on glass substrates grown by chambers with background vacuum of 10^{-3} and 10^{-7} Pa, respectively. The oxygen anion composition of ZTNO thin films is also plotted as a function of Zn/(Zn + Sn) (authors' original work).

Considering quite a little O content of ZTN thin films grown in the UHV chamber, this seems to indicate that the sole Zn cation engineering cannot tune the ρ of ZTN thin films notably.

On the contrary, the resistivities of ZTNO increase significantly, from 0.38 (Zn/(Zn + Sn) ~ 0.53) to 2.91×10^5 Ω·cm (Zn/(Zn + Sn) ~ 0.65) when increasing the Zn/(Zn + Sn) compositions, as shown in Figure 6. Taking the ZTNO ~ 0.65 Zn/(Zn + Sn) thin film as an example, its resistivity even exceeds the 9.91×10^3 Ω·cm of ZnO thin film deposited in the same chamber. Unfortunately, its n and μ_H cannot be identified precisely due to the large noise level for such ZTNO thin films with rich Zn compositions. The O content of ZTNO thin films as a function of Zn/(Zn + Sn) composition is also plotted in Figure 6, which shows similar evolution tendency to ρ of ZTNO. This means the high ρ of ZTNO with rich Zn cations is accompanied by the large amount of O anions. Comparing the electrical properties and O compositions of ZTN and ZTNO thin films, it is demonstrated that the joint incorporation of excess O and Zn compositions reduces n effectively.

Finally, microstructures and spatial distribution of ZTNO and ZTN thin films have been investigated. Figure 7(a) shows a scanning transmission electron microscopy (STEM) top-view image of highly resistive ZTNO thin film with 0.65 Zn/(Zn + Sn) composition, indicating grain sizes of less than 20 nm. Figure 6(b) exhibits EDS line profile analyses of Sn, Zn, O and N elements in the selected region marked by the red line in Figure 7(a). As seen in the bottom panel of Figure 7(b), N distributes homogeneously in ZTNO thin film, whereas the elements of Sn, Zn and O are inhomogeneous. Looking at Sn and Zn, their content evolutions as a function of position surprisingly show opposite tendency. As shown in Figure 7(b), the region with low amount of Sn contains high content of Zn. In addition, O possesses the similar evolution tendency to that of Zn, which seems to indicate that locally inhomogeneous ZnO grains also exist in the Zn- and O-rich regions in ZTNO thin film. Coincidentally, this is consistent with crystal features determined by the XRD patterns in Figure 5. On the contrary, the STEM and EDS line profile analyses of ZTN thin films do not show such non-homogeneous distributions of elements, as shown in Figure 7(c) and (d).

The tunable electrical properties of ZTNO thin films by O and Zn composition shown in Figure 6 can be understood from the viewpoints of the theoretical defect properties and the microstructure of thin film. The defect properties of oxynitride ZTNO have been investigated using the first-principle calculations by Pan et al. [29]. It is demonstrated that the defect complexes, like $(Zn_{Sn} + 2O_N)^0$,

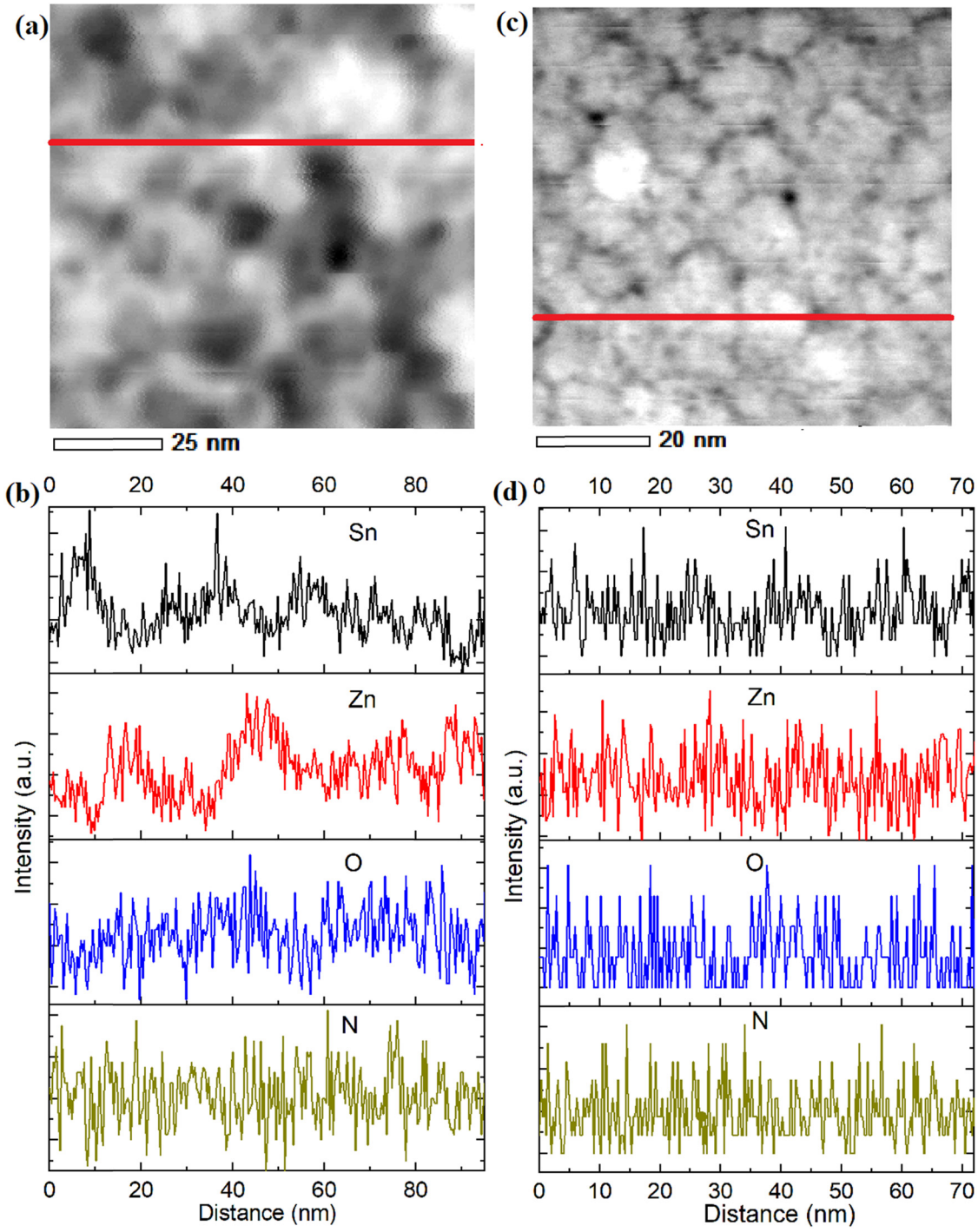

Figure 7: (a) and (b) are STEM image and EDS line profile analyses of ZTNO thin film on Si (100) substrate with 0.65 Zn/(Zn + Sn) composition, respectively. (c) and (d) are STEM image and EDS line profile analyses of ZTN thin film on Si (100) substrate with 0.72 Zn/(Zn + Sn) composition, respectively. The red lines in (a) and (c) represent the selected regions for EDS line profile analyses (authors' original work).

are of great importance to tune *n*. These stable defect complexes are composed of defects with opposite charges, such as Zn_{Sn}^{-2} and O_N^+, leading to a coupling between O incorporation and Zn cation stoichiometry. Such association between Zn_{Sn}^{-2} and O_N^+ is exothermic and drastically decreases the formation energy of acceptor-type Zn_{Sn}^{-2} defects, which can compensate the donor-type Sn_{Zn}^{2+}, O_N^+ and V_N^+ defects significantly [29]. This is consistent with our experimental result

that the incorporation of O into Zn-rich thin films produces much higher ρ (Figure 6). Experimentally, Fioretti et al. [34] identified a defect complex ($Zn_{Sn} + 2O_N$)-related excitonic photoluminescence (PL) by low temperature (4 K) PL characterizations with various excitation powers [34]. In addition, the defect complexes composed of Zn_{Sn}^{-2} and H_i^+, such as $(Zn_{Sn} + 2H_i)^0$, may also contribute to the compensation of donor-type H_i^+ defects, as predicted by the first principle calculations [27]. Such type of association is quite similar to that between Zn_{Sn}^{-2} and O_N^+, yielding the joint effects on the compensation of donor-type defects. Besides, the co-existence of ZTN and ZnO nanograins in Zn-rich ZTNO thin films is also beneficial to yield a high ρ (Figure 7), as ZnO grains may possess much higher ρ and there are more interfacial scattering between ZTN and ZnO grains. Due to the quite close crystallographic features of orthorhombic ZTN and wurtzite ZnO, the co-existence of ZTN and ZnO in ZTNO thin films can also be described as alloying. Here it is worth noting that the amounts of ZnO grains in ZTNO thin films should be very low, as the optical band gap of 1.53 eV of ZTNO ~0.65 Zn/(Zn + Sn) thin film is quite close to the 1.32 eV of ZTN ~ 0.72 Zn/(Zn + Sn) thin film.

6 Conclusion

In this work, we demonstrated the electrical measurements of ZN and ZTN thin films deposited at low growth temperature. It is shown that the low temperature deposition is beneficial to suppress the carrier concentrations of ZN and ZTN thin films, giving rise to non-degenerate electrical conductivity. Theoretical analyses of defect properties of ZN demonstrate that unintentional oxygen-on-nitrogen (O_N^+) and/or hydrogen interstitial (H_i^+) defects act as dominant donors, which are responsible for the high carrier concentration in ZN thin films. The concentration of O_N^+/H_i^+ exhibits a significant dependence on temperature, as these types of defects follow the Boltzmann distribution. Besides, Zn-rich content is also useful to reduce the carrier concentration, which indicates that excess Zn content can reduce the amount of native donor-type Sn_{Zn}^{2+} defects. Combining the excess Zn content and the low temperature growth in ZTN, non-degenerate thin films with high mobility can be achieved by a UHV growth chamber.

In addition, the electrical properties of ZTN thin films can also be tuned by combining the rich Zn and O compositions. It is found that the Zn-rich ZTN thin films incorporated with more O content grown in a chamber with the poor background vacuum of 10^{-3} Pa possess much higher resistivities than those deposited by a UHV chamber with background vacuum of 10^{-7} Pa. These results seem to demonstrate that combining the rich Zn and O compositions together in ZTN thin films can suppress the carrier concentration significantly. These electrical properties are in good accordance with the recently theoretical calculation on the defect properties of ZTN, which indicates that the defect complexes (like $(Zn_{Sn} + 2O_N)^0$) are of great importance to tune the carrier concentrations. The association between Zn_{Sn}^{-2} and O_N^+ in these stable complexes will reduce the formation energy of acceptor-type Zn_{Sn}^{-2} defects dramatically, which could compensate the donor-type defects and increase the resistivity remarkably. These results may provide a general framework for controlling the carrier concentration in novel nitride semiconductors toward photovoltaic applications.

Acknowledgments: Y. Wang would like to acknowledge the funding from NIMS-ICYS (No. QN3140), the Open Project of State Key Laboratory of Environment-friendly Energy Materials (19kfhg14) and the Qilu Young Scholar at Shandong University.

Funding information: NIMS-ICYS (No. QN3140), the Open Project of State Key Laboratory of Environment-friendly Energy Materials (19kfhg14) and the Qilu Young Scholar at Shandong University.

Author contributions: Y.W. carried out main parts of the work and wrote the first version of this paper. Y.W. directed the study. T.O. contributed to partial experiments and lots of analyses for the results. F.A. and J.P. contributed to the partial experiments and discussion. N.O. provided the resources and contributed to the discussion. All authors commented on the manuscript.

Conflicts of interest: Authors state no conflict of interest.

Data availability statement: The data that support the findings of this study are available from the corresponding author upon reasonable request.

References

[1] Kumagai, Y., K. Harada, H. Akamatsu, K. Matsuzaki, and F. Oba. Carrier-induced band-gap variation and point defects in Zn_3N_2 from first principles. *Physical Review Applied*, Vol. 8, No. 1, 2017, id. 014015.

[2] Hinuma, Y., T. Hatakeyama, Y. Kumagai, L. A. Burton, H. Sato, Y. Muraba, et al. Discovery of earth-abundant nitride semiconductors by computational screening and high-pressure

synthesis. *Nature Communications*, Vol. 7, No. 1, 2016, id. 11962.

[3] Shockley, W. and H. J. Queisser. Detailed balance limit of efficiency of *p-n* junction solar cells. *Journal of Applied Physics*, Vol. 32, No. 3, 1961, pp. 510–519.

[4] Suda, T. and K. Kakishita. Band-gap energy and electron effective mass of polycrystalline Zn_3N_2. *Journal of Applied Physics*, Vol. 99, No. 7, 2006, id. 076101.

[5] Maile, E. and R. A. Fischer. MOCVD of the cubic zinc nitride phase, Zn_3N_2, using Zn[N(SiMe3)2]2 and ammonia as precursors. *Chemical Vapor Deposition*, Vol. 11, No. 10, 2005, pp. 409–414.

[6] Trapalis, A., J. Heffernan, I. Farrer, J. Sharman, and A. Kean. Structural, electrical, and optical characterization of as grown and oxidized zinc nitride thin films. *Journal of Applied Physics*, Vol. 120, No. 20, 2016, id. 205102.

[7] Núñez, C. G., J. L. Pau, M. J. Hernández, M. Cervera, E. Ruiz, and J. Piqueras. On the zinc nitride properties and the unintentional incorporation of oxygen. *Thin Solid Films*, Vol. 520, No. 6, 2012, pp. 1924–1929.

[8] Cao, X., Y. Yamaguchi, Y. Ninomiya, and N. Yamada. Comparative study of electron transport mechanisms in epitaxial and polycrystalline zinc nitride films. *Journal of Applied Physics*, Vol. 119, No. 2, 2016, id. 025104.

[9] Feldberg, N., J. D. Aldous, W. M. Linhart, L. J. Phillips, K. Durose, P. A. Stampe, et al. Growth, disorder, and physical properties of $ZnSnN_2$. *Applied Physics Letters*, Vol. 103, No. 4, 2013, id. 042109.

[10] Lahourcade, L., N. C. Coronel, K. T. Delaney, S. K. Shukla, N. A. Spaldin, and H. A. Atwater. Structural and optoelectronic characterization of RF sputtered $ZnSnN_2$. *Advanced Materials*, Vol. 25, No. 18, 2013 May 14, pp. 2562–2566.

[11] Makin, R. A., K. York, S. M. Durbin, and D. Lorraine. F.- Nancy, and R. J. Reeves. Alloy-free band gap tuning across the visible spectrum. *Physical Review Letters*, Vol. 122, 2019, id. 256403.

[12] Han, L., C. Lieberman, and H. Zhao. Study of intersubband transitions in GaN-$ZnGeN_2$ coupled quantum wells. *Journal of Applied Physics*, Vol. 121, 2017, id. 093101.

[13] Karim, R., B. Hewage, D. Jayatunga, Z. Feng, K. Kash, and H. Zhao. Metal–organic chemical vapor deposition growth of $ZnGeN_2$ films on sapphire. *Crystal Growth & Design*, Vol. 19, No. 8, 2019, pp. 4661–4666.

[14] Skachkov, D., A. P. Jaroenjittichai, L. Huang, and W. R. L. Lambrecht. Native point defects and doping in $ZnGeN_2$. *Physical Review. B*, Vol. 93, No. 15, 2016, id. 155202.

[15] Veal, T. D., N. Feldberg, N. F. Quackenbush, W. M. Linhart, D. O. Scanlon, L. F. J. Piper, et al. Band gap dependence on cation disorder in $ZnSnN_2$ solar absorber. *Advanced Energy Materials*, Vol. 5, No. 24, 2015, id. 1501462.

[16] Karim, M. R. and H. Zhao. Design of InGaN-$ZnSnN_2$ quantum wells for high-efficiency amber light emitting diodes. *Journal of Applied Physics*, Vol. 124, No. 3, 2018, id. 034303.

[17] Narang, P., S. Chen, N. C. Coronel, S. Gul, J. Yano, L. W. Wang, et al. Bandgap tunability in $Zn(Sn,Ge)N_2$ semiconductor alloys. *Advanced Materials*, Vol. 26, No. 8, 2014, pp. 1235–1241.

[18] Quayle, P. C., E. W. Blanton, A. Punya, G. T. Junno, K. He, L. Han, et al. Charge-neutral disorder and polytypes in heterovalent wurtzite-based ternary semiconductors: The importance of the octet rule. *Physical Review B: Condensed Matter and Materials Physics*, Vol. 91, No. 20, 2015, id. 205207.

[19] Lany, S., A. N. Fioretti, P. P. Zawadzki, L. T. Schelhas, E. S. Toberer, A. Zakutayev, et al. Monte Carlo simulations of disorder in $ZnSnN_2$ and the effects on the electronic structure. *Physical Review Materials*, Vol. 1, No. 3, 2017, id. 035401.

[20] Qin, R., H. Cao, L. Liang, Y. Xie, F. Zhuge, H. Zhang, et al. Semiconducting $ZnSnN_2$ thin films for Si/$ZnSnN_2$ p-n junctions. *Applied Physics Letters*, Vol. 108, No. 14, 2016, id. 142104.

[21] Feldberg, N., B. Keen, J. D. Aldous, D. O. Scanlon, P. A. Stampe, R. J. Kennedy, et al. *Conference Record of the IEEE Photovoltaic Specialists Conference*, 2021, p. 002524.

[22] Fioretti, A. N., A. Zakutayev, H. Moutinho, C. Melamed, J. D. Perkins, A. G. Norman, et al. Combinatorial insights into doping control and transport properties of zinc tin nitride. *Journal of Materials Chemistry C, Materials for Optical and Electronic Devices*, Vol. 3, No. 42, 2015, pp. 11017–11028.

[23] Kawamura, F., N. Yamada, X. Cao, M. Imai, and T. Taniguchi. The bandgap of $ZnSnN_2$ with a disordered-wurtzite structure. *Japanese Journal of Applied Physics*, Vol. 58, 2019, id. SC1034. Doi: 10.7567/1347-4065/ab0ace.

[24] Fioretti, A. N., A. Zakutayev, H. Moutinho, C. Melamed, J. D. Perkins, A. G. Norman, et al. Combinatorial insights into doping control and transport properties of zinc tin nitride. *Journal of Materials Chemistry. C, Materials for Optical and Electronic Devices*, Vol. 3, No. 42, 2015, pp. 11017–11028.

[25] Alnjiman, F., S. Diliberto, J. Ghanbaja, E. Haye, S. Kassavetis, P. Patsalas, et al. Chemical environment and functional properties of highly crystalline $ZnSnN_2$ thin films deposited by reactive sputtering at room temperature. *Solar Energy Materials and Solar Cells*, Vol. 182, 2018, pp. 30–36.

[26] Cao, X., F. Kawamura, Y. Ninomiya, T. Taniguchi, and N. Yamada. Conduction-band effective mass and bandgap of $ZnSnN_2$ earth-abundant solar absorber. *Scientific Reports*, Vol. 7, No. 1, 2017 Nov 8, id. 14987.

[27] Tsunoda, N., Y. Kumagai, A. Takahashi, and F. Oba. Electrically benign defect behavior in zinc tin nitride revealed from first principles. *Physical Review Applied*, Vol. 10, No. 1, 2018, id. 011001.

[28] Wang, Y., T. Ohsawa, X. Meng, F. Alnjiman, J. F. Pierson, and N. Ohashi. Suppressing the carrier concentration of zinc tin nitride thin films by excess zinc content and low temperature growth. *Applied Physics Letters*, Vol. 115, No. 23, 2019, id. 232104.

[29] Pan, J., J. Cordell, G. J. Tucker, A. C. Tamboli, A. Zakutayev, and S. Lany. Interplay between composition, electronic structure, disorder, and doping due to dual sublattice mixing in nonequilibrium synthesis of $ZnSnN_2$:O. *Advanced Materials*, Vol. 31, No. 11, 2019, id. 1807406.

[30] Hamilton, D. C., E. Arca, J. Pan, S. Siol, M. Young, S. Lany, et al. Electron scattering mechanisms in polycrystalline sputtered zinc tin oxynitride thin films. *Journal of Applied Physics*, Vol. 126, No. 3, 2019, id. 035701.

[31] Wang, Y., T. Ohsawa, Y. Kumagai, K. Harada, F. Oba, and N. Ohashi. Achieving non-degenerate Zn_3N_2 thin films by near room temperature sputtering deposition. *Applied Physics Letters*, Vol. 115, No. 9, 2019, id. 092104.

[32] Kumagai, Y., K. Harada, H. Akamatsu, K. Matsuzaki, and F. Oba. Carrier-induced band-gap variation and point defects

in Zn_3N_2 from first principles. *Physical Review Applied*, Vol. 8, No. 1, 2017, id. 014015.

[33] Lany, S. Band-structure calculations for the 3d transition metal oxides in G W. *Physical Review B: Condensed Matter and Materials Physics*, Vol. 87, No. 8, 2013, id. 085112.

[34] Fioretti, A. N., J. Pan, B. R. Ortiz, C. L. Melamed, P. C. Dippo, L. T. Schelhas, et al. Exciton photoluminescence and benign defect complex formation in zinc tin nitride. *Materials Horizons*, Vol. 5, No. 5, 2018, pp. 823–830.